

# Preparation and *In Vitro* Drug Release Behavior of 1,10-Phenanthroline/ $\beta$ -cyclodextrin–poly (Glycidyl Methacrylate) Drug-Loaded Microspheres

Ya Li and Weijun Zhen\*

Key Laboratory of Oil and Gas Fine Chemicals, Ministry of Education and Xinjiang Uygur Autonomous Region, Xinjiang University, Urumqi 830046, China

**Abstract:** In this study, novel star-shaped polymers of  $\beta$ -cyclodextrin ( $\beta$ -CD)–poly (glycidyl methacrylate) (PGMA) were prepared by atom transfer radical polymerization (ATRP), formed from GMA and  $\beta$ -CD. In addition, the structure, properties and hydrophilicity of the  $\beta$ -CD-PGMA polymers thus prepared were systematically analyzed. 1,10-phenanthroline monohydrate (Phen)/ $\beta$ -CD-PGMA drug-loaded microspheres were prepared by emulsion solvent evaporation. The optimum preparation conditions were determined by orthogonal tests. Analysis results indicated that the performance of star-shaped polymers of  $\beta$ -CD-PGMA clearly changes, resulting in the increase of the contact angle from 17° to 72.5°, and their thermal degradation temperature was enhanced from 260 °C to 401 °C. Moreover,  $\beta$ -CD-PGMA drug-loaded microspheres with a smooth, spherical surface were successfully prepared, and the drug-loading capacity and average particle size of drug-loaded microspheres were 26.67 % and 10  $\mu$ m, respectively. Drug release tests indicated that the release behavior of  $\beta$ -CD-PGMA drug-loaded microspheres conformed to Higuchi release kinetics, which exhibited a significant drug delivery capability. The release rate and utilization of  $\beta$ -CD-PGMA were greater than that of  $\beta$ -CD, demonstrating that  $\beta$ -CD-PGMA was more suitable as a drug delivery material.

**Keywords:**  $\beta$ -cyclodextrin, glycidyl methacrylate, atom transfer radical polymerization, drug-loaded microspheres, star-shaped polymers, release kinetics.

## 1. INTRODUCTION

With the demand of highly efficient drugs, increasing attention has been focused on drug delivery using biomedical materials exhibiting low cytotoxicity and high release efficiency [1-4]. Recently, a large number of polycations, including polylactic acid (PLA) [5], polycaprolactone (PCL) [6], cyclodextrin (CD) [7], polyethylene glycol (PEG) [8], poly(tertiary amine methacrylate) [9], polyvinyl phosphonic acid (PVPA) [10], glycidyl methacrylate (GMA) [11], poly(N-isopropylacrylamide) (PNIPAM) [12] have been reported for drug delivery in biomaterials and biomedical applications. CDs are a series of cyclic oligosaccharides composed of six, seven, or eight D(+)-glucose units linked by  $\alpha$ -1,4-linkages, referred to as  $\alpha$ -,  $\beta$ -, or  $\gamma$ -CD, respectively [13-15], which exhibit certain hydrophilicity and environmental friendliness. Hence, CDs are widely used as drug carriers. Local drug administration and release from matrices can be affected by the presence of CDs, sometimes protection effect of the included/conjugated drugs from deactivation [16, 17].

However, in most cases, the release of the drug from CDs is rapid [18]. For overcoming this

shortcoming, a modified group was introduced into CDs for prolonging the release time. The hydroxyl groups in CDs afford facile polysubstitution as esterification provides mature, reliable methods for further decoration [19]. Simultaneously, in the past few years, the preparation of modified CDs has attracted significant attention. For instance, Shi *et al.* [20] and Huang *et al.* [21] have reported the preparation of linear polymers by modified CDs, where the release rate is controlled by adjusting the pH or degree of network.

Nevertheless, star-shaped polymers have recently attracted considerable attention as drug carriers owing to its dense molecular structure with moderate flexibility [22]. Moreover, they have been widely used as model branched polymers for evaluating the effect of segment density and chain topology on polymer properties [23, 24]. Typically, star-shaped polymers are synthesized by two major pathways: “core-first” and “arm-first” approaches [24, 25]. Because CDs have a unique steric structure with a truncated cone [25], novel star-shaped drug carriers with CDs as cores are synthesized and the hydroxyl groups on the outside surfaces of CDs are served as initiation sites for growing cationic branches [26, 22]. GMA has been used in DNA separation, enzyme immobilization, and targeted drug delivery etc. [5]. The presence of the oxirane group in GMA and its copolymers favors further chemical modification for various applications [26].

\*Address correspondence to this author at the Key Laboratory of Oil and Gas Fine Chemicals, Ministry of Education and Xinjiang Uygur Autonomous Region, Xinjiang University, Urumqi 830046, China; Tel/Fax: 86-991-8582078; E-mail: zhenweijun6900@163.com

Because conventional radical polymerization is easy to break oxirane group of GMA, the synthesis of GMA employs some novel schemes. Among of them, ATRP is a very promising controlled radical polymerization (CRP) technique, affording polymers with well-defined molecular weights and narrow molecular weight distribution under mild reaction conditions [26, 27]. Above all, ATRP is a type of an extended chain reaction without the destruction of the ether bond [26].

In this study, star-shaped polymers of  $\beta$ -CD-PGMA were prepared by ATRP. Then, 1,10-phenanthroline monohydrate (Phen) was used for conducting experiments with the drug-loaded microspheres of the polymers, and the factors affecting the formation of microspheres were investigated. Because of its solubility in several organic compounds, Phen was suitable as a template drug. Drug release behavior as well as release kinetics of  $\beta$ -CD-PGMA microspheres were investigated.

## 2. EXPERIMENTAL

### 2.1. Materials

$\beta$ -cyclodextrin ( $\beta$ -CD, >98%), vacuum-dried overnight before use, was obtained from Sanpu Chemical Co., Ltd., Shanghai, China. GMA (>98%), 2-bromoisobutyrate bromide (BIBB, >99%), copper(I) bromide (CuBr, >99%), copper(II) bromide (CuBr<sub>2</sub>, >99%), triethylamine (TEA, >99%), N,N-dimethylformamide (DMF, >99%), N,N-dimethylacetamide (>99%) and 2,2'-bipyridine (Bpy, 99%) were purchased from J&K Scientific Chemical Co., China. Polyvinyl alcohol (17–88; degree of polymerization, 1750  $\pm$  50; hydrolysis degree, 87%–89%) was purchased from Chengdu Kelong Chemical Plant, China. 1,10-phenanthroline monohydrate (>99.5%) was obtained from Tianjin Fine Chemical Development Center, Tianjin, China. A dialysis membrane bag ( $M_w$  = 8000–14000 g/mol) was obtained from Solarbio Biological Technology Co., Ltd, Beijing, China. Dichloromethane, tetrahydrofuran (THF), dimethyl sulfoxide, aluminum oxide, and acetone were used without further purification.

Figure 1 shows the synthesis scheme of  $\beta$ -CD-PGMA.

### 2.2. Preparation of Macromolecular Initiator $\beta$ -CD-Br

Firstly,  $\beta$ -CD (2.25 mmol) was completely dissolved in 15 mL of anhydrous DMF with stirring and then

placed in an ice bath, followed by the addition of 1.8 mL BIBB and 1.8 mL TEA. Second, the reaction mixture was gently stirred for another 2 h at 0 °C in an ice-water bath and flushed with nitrogen at room temperature for 24 h. Thirdly, the final reaction mixture was precipitated using diethyl ether. The white powder precipitate was collected by centrifugation and washed using acetone. The crude product was purified by suspending it in 100 mL of deionized water at room temperature overnight. The purified CD-Br was collected by suction filtration, washed with acetone, and dried under reduced pressure at 40 °C.

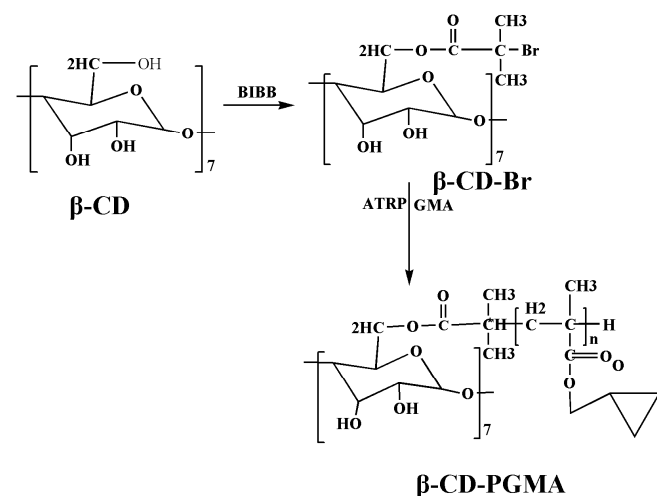


Figure 1: The synthesis scheme of  $\beta$ -CD-PGMA.

### 2.3. Preparation of Star-Shaped Polymers of $\beta$ -CD-PGMA by ATRP

$\beta$ -CD-PGMA star polymers were synthesized by ATRP. ATRP conditions were optimized according to an orthogonal experimental procedure (Table 1). The reaction was performed in a 50 mL flask equipped with a magnetic stirrer under conditions typical for ATRP. Firstly, CD-Br, DMF, GMA and Bpy were added into a flask containing a 10 mL DMF mixture. Secondly, after CD-Br was completely dissolved, the reaction mixture was degassed with nitrogen for 10 min. Thirdly, CuBr and CuBr<sub>2</sub> were added into the mixture under nitrogen. Next, the reaction mixture was purged with nitrogen for another 30 min. The flask was then sealed with a rubber stopper under nitrogen gas. Polymerization was allowed to proceed under continuous stirring at 40 °C for several hours. The reaction was stopped by diluting with THF, and the catalyst complex was removed by passing the blue dilute polymer solution through a short aluminum oxide column. A colorless solution was obtained. After removing THF using a rotary evaporator,  $\beta$ -CD-PGMA was precipitated using excess

acetone. Finally, the crude polymer was purified by reprecipitation two times in acetone for removing the reactant residues, prior to being dried under reduced pressure at 40 °C.

#### 2.4. Preparation of $\beta$ -CD-PGMA Drug-Loaded Microspheres

Firstly,  $\beta$ -CD-PGMA drug-loaded microspheres were prepared by oil/water (O/W) emulsion solvent evaporation. A phen-saturated aqueous solution with a certain concentration of PVA1788 as the water phase and an appropriate amount of  $\beta$ -CD-PGMA and Phen dissolved in the mixture as the oil phase ([dichloromethane]/[sulfoxide] in a ratio of 9:1 (v:v)) under ultrasonic radiation for 20 min at room temperature. The oil phase with a syringe slowly dripped into the water phase under mechanical stirring for certain time after dropping. The final mixture was separated by high-speed centrifugation and washed three times with distilled water for precipitation, and dried under reduced pressure at 40 °C.

#### 2.5. Preparation of Phen/ $\beta$ -CD Microspheres

Drug-loaded microspheres of  $\beta$ -CD were prepared by water/oil/ (W/O) emulsion solvent evaporation. Firstly,  $\beta$ -CD and a 40 wt% sodium hydroxide solution were added into three-neck flask under mechanical agitation. Secondly, after the mixture was stirred at 50 °C, 12.5 mL of epichlorohydrin was added dropwise in 20 min at 30 °C and stirred at 800 rpm for another 1.5 h. Thirdly, 80 g kerosene containing 3 wt% emulsifier (Span 80:Tween 20 = 3:1) was slowly dripped into the mixture under high-speed stirring. Next, after stirring for 10 min, stirring speed and reaction temperature were changed to 800 rpm and 50 °C, respectively. This process was allowed to proceed under continuous stirring at 50 °C for 6 h. The final reaction mixture was allowed to stand, and the upper oil phase was decanted. The microspheres were collected by centrifugation, sufficiently washed with dilute hydrochloric acid, ethanol, distilled water, and acetone in the order stated, followed by drying under reduced pressure at 40 °C.

#### 2.6. Test Method for Drug Loading and Drug Release Properties of Phen/ $\beta$ -CD-PGMA Microspheres

A series of standard solutions with different concentrations were prepared using Phen in a phosphate buffer solution (PBS, pH = 7.4, 0.1 mol/L). Using a PBS solution as the reference liquid, the

absorbance (A) of the standard solution was determined by UV–VIS spectrophotometry at a wavelength of 323 nm. The calibration curve of Phen was obtained:  $A = 0.00301C - 0.00951$ ,  $R^2 = 0.99972$ ; linear range from 18 to 300 mg/mL.

A specific amount of Phen/ $\beta$ -CD-PGMA microspheres was added to 5 mL of a solution (volume ratio [dichloromethane]/ [sulfoxide] of 9:1 (v:v)) and subjected to ultrasonication for enabling complete dissolution. Then, the  $\beta$ -CD-PGMA sediment was completely separated by the addition of quantitative deionized water. The absorbance of the supernatant after centrifugation was determined at  $\lambda = 323$  nm. Formula (1) and (2) show drug loading and drug entrapment efficiency, respectively.

$$\text{Drug loading (\%)} = (\text{Drug quality of microspheres} / \text{Microsphere quality}) \times 100\% \quad (1)$$

$$\text{Drug entrapment efficiency (\%)} = (\text{Drug quality of microspheres} / \text{Drug quality}) \times 100\% \quad (2)$$

The *in vitro* drug release behavior of drug-loaded microspheres was determined by dynamic membrane dialysis. Specific amounts of Phen/ $\beta$ -CD-PGMA, Phen/ $\beta$ -CD, and Phen particles were added in a 50 mL PBS solution at 37 °C in a dialysis membrane bag. Then, a 3 mL solution was utilized for measuring absorbance, and an equal volume of the same dissolution medium was added for maintaining a constant volume at regular intervals. The concentration of Phen in the sample solution was calculated using the calibration curve of Phen, and the cumulative release percentage of the drug in the sample was calculated by formula (3).

$$\text{Cumulative release percentage (\%)} = (\text{release drug quality} / \text{theory of drug quality}) \times 100\% \quad (3)$$

#### 2.7. Characterization and Testing

The chemical composition of  $\beta$ -CD-PGMA star-shaped polymers was determined by X-ray photoelectron spectroscopy (XPS). XPS measurements were conducted on an XPS system (Axis Ultra, Kratos Analytical, Britain) with a monochromatized AlK $\alpha$  X-ray source (284.7 eV). All binding energies (BEs) were referenced to the C1s hydrocarbon peak at 284.7 eV. Atomic concentrations of each element were calculated from integral peak intensities using a linear background. The systematic error was on the order of 3–5 %.

The Fourier transform infrared spectra (FTIR) of samples were recorded on a Bruker Equinox 55 (Germany) FTIR spectrometer by the standard KBr pellet disc technique. Spectra were collected from 4000 to 400  $\text{cm}^{-1}$  at a resolution of 4  $\text{cm}^{-1}$ .

$^1\text{H}$  NMR spectra were recorded on an INOVA 400 MHz spectrometer (Varian, Co., LTD, USA) at 400 MHz in dimethyl sulfoxide ( $\text{DMSO-d}_6$ ) at room temperature.

The hydrophilicity of  $\beta$ -CD-PGMA star-shaped polymers was estimated using a contact angle meter (JJ2000B2, Zhongchen Digital Technology Co., China). The specimens were pressed into small sheets with a thickness of approximately 2 mm using an SSP-10-type tablet press before testing. Prior to testing, all samples were dried to constant weight at 40  $^\circ\text{C}$  in a vacuum oven.

Thermogravimetric analysis was conducted on an SDT-Q600 TGA system (USA). Samples (approximately 5–10 mg) were subjected to at a heating rate of 10  $^\circ\text{C}/\text{min}$  at temperatures ranging from room temperature to 500  $^\circ\text{C}$  with nitrogen (100 mL/min) as the purge gas.

Differential scanning calorimetry (DSC) thermograms of the samples (approximately 5–8 mg) were recorded on a DSC Q2000 system (USA). Samples were performed by heating from room temperature to 180  $^\circ\text{C}$  at a heating rate of 10  $^\circ\text{C}/\text{min}$  under a nitrogen flow (40 mL/min).

Raman spectra of the samples were recorded on a Senterra microscope (Germany Bruker CO.) Spectra were collected in the region from 2000  $\text{cm}^{-1}$  to 100  $\text{cm}^{-1}$  at a laser wavelength of 785 nm, laser power of 50 mW, and with a laser-light-focused spot range of 50  $\times$  1000  $\mu\text{m}$ .

The morphology of the microspheres was observed on a scanning electron microscope (SEM, Inspect F, FEI Instrument Co., Ltd, The Netherlands) at an acceleration voltage of 20 kV. Prior to SEM evaluation, the sample was sputter-coated using gold for preventing charging.

### 3. RESULTS AND DISCUSSION

#### 3.1. Orthogonal Optimization for the Preparation of $\beta$ -CD-PGMA Star-Shaped Polymers

For optimizing the preparation of  $\beta$ -CD-PGMA star-shaped polymers, the water contact angle was used as

the objective function. The molar feed ratio of GMA/ $\beta$ -CD-Br (A), the molar ratio of CuBr/CuBr<sub>2</sub>/Bpy (B), reaction temperature (C) and reaction time (D) were selected as the four effect factors as the object of the orthogonal experiment. By the orthogonal design experiment of L<sub>9</sub> (3<sup>4</sup>) (Table 1), optimum conditions were selected, and the water contact angle was evaluated on the basis of the optimum conditions.

**Table 1: Factor Level of the Orthogonal Experiment L<sub>9</sub> (3<sup>4</sup>) for the Preparation of  $\beta$ -CD-PGMA**

Level	Factors			
	A (mmol)	B (mmol)	C ( $^\circ\text{C}$ )	D (h)
1	80	3:0.75:3.6	25	3
2	120	4:1:4.8	40	5
3	160	5:1.25:6	65	8

**Table 2: Results Obtained from the Orthogonal Experiment for the Preparation of  $\beta$ -CD-PGMA**

NO.	Factors				Water contact angle ( $^\circ$ )
	A	B	C	D	
1	1	1	1	1	47.1
2	1	2	2	2	51.4
3	1	3	3	3	49.0
4	2	1	2	7	62.0
5	2	2	3	1	60.0
6	2	3	1	2	54.5
7	3	1	3	2	50.5
8	3	2	1	3	50.8
9	3	3	2	1	47.1
K <sub>1</sub>	49.2	53.2	50.8	51.4	
K <sub>2</sub>	58.8	54.0	53.5	52.1	
K <sub>3</sub>	49.5	50.2	53.2	53.9	
R	9.7	3.8	2.7	2.5	

Effects of factors on experimental results: A > B > C > D; Optimum conditions: A<sub>2</sub>B<sub>2</sub>C<sub>2</sub>D<sub>3</sub>.

Table 2 shows the results obtained from the orthogonal experiments with  $\beta$ -CD-PGMA. By the comparison range of each factor, the factors affecting the water contact angle were in the following order: molar feed ratio of GMA/ $\beta$ -CD-Br (A) > molar ratio of CuBr/CuBr<sub>2</sub>/Bpy (B) > reaction temperature (C) > reaction time (D). From Table 2, at a constant  $\beta$ -CD-Br amount, the water contact angle of  $\beta$ -CD-PGMA star-shaped polymers increased with increasing amount of GMA monomer. With increasing amount of GMA

monomer, side effects occurred to block polymerization. With a low CuBr amount, the reaction proceeded more slowly, indicating that reaction exhibited low activity. In turn, the self-polymerization of GMA monomer was carried out. At low temperature, the reaction proceeded more slowly. In turn, side reactions increased with increasing temperature. As the ATRP reaction was controlled, the grafting yield increased with time. However, after the reaction reached a certain degree, the yield was constant as time progressed.

Hence, the results obtained from orthogonal experiments indicating that the optimum conditions of drug loading were a molar feed ratio of 120 for GMA/ $\beta$ -CD-Br, molar ratio of CuBr/CuBr<sub>2</sub>/Bpy of 4:1:4.8, reaction temperature of 40 °C, and a reaction time of 8 h. Finally, under optimum conditions, the water contact angle of  $\beta$ -CD-PGMA was 72.5° (Figure 2b).

### 3.2. Water Contact Angle Test

By determining the contact angle on the surface of liquid (water) in the samples and comparing their wettability with the liquid, macroscale differences of sample surface properties become evident [30]. Figure 2 shows the images obtained for the contact angles of the interface between  $\beta$ -CD and  $\beta$ -CD-PGMA star-shaped polymers. The contact angles of pure  $\beta$ -CD and  $\beta$ -CD-PGMA star-shaped polymers were 17° and 72.5°, respectively. As each  $\beta$ -CD has several hydrophilic hydroxyl groups,  $\beta$ -CD has high hydrophilicity. After grafting, the hydrophilicity of modified  $\beta$ -CD was weakened because the  $\beta$ -CD-PGMA polymers on the whole were hydrophobic attributed to the fact that the PGMA branches consist of ester and ether bonds. Thus,  $\beta$ -CD-PGMA polymers inhibit the adsorption of water but exhibit other favorable properties.

### 3.3. XPS Analysis

For gaining insight into the interaction between the immobilization of the ATRP initiator BIBB and  $\beta$ -CD, XPS analysis was performed for analyzing the chemical composition of  $\beta$ -CD-Br.

Figure 3 presents the XPS surveys of  $\beta$ -CD-Br. The photoelectron peaks at 532 eV and 285 eV in wide scan respond to the O 1s and C 1s orbits, respectively. Figure 3b and 3c show the XPS C 1s binding energy spectrum of  $\beta$ -CD-Br and the corresponding Br 3d binding energy spectrum, respectively. According to the study [13], the C 1s core-level spectrum of CD-Br was curve-fitted by four peak components with BEs of approximately 284.7, 285.5, 286.4 and 288.7 eV, corresponding to the C-H/C-C, C-O/C-Br, O-C-O and O=C-O species, respectively [31]. The unambiguous O-C=O peak component represented the bromide-capped ester groups of CD-Br. The Br 3d signal at binding energy of about 70 eV, characteristic of covalently bonded bromine, was also shown in Figure 3c. The XPS results indicated that a CD-Br core is successfully prepared.

### 3.4. FTIR Analysis

Figure 4 shows the FTIR spectra of raw  $\beta$ -CD, GMA, and  $\beta$ -CD-PGMA star-shaped polymers. As can be observed from Figure 4, spectral features for the  $\beta$ -CD-PGMA polymers indicated not only  $\beta$ -CD functional group peak but also that of GMA, where a characteristic infrared peak was observed at 912 cm<sup>-1</sup>, corresponding to the ether linkage. The peak corresponding to the carbon-carbon double bond of GMA at 1640 cm<sup>-1</sup> disappeared, and as compared with that of non-modified  $\beta$ -CD, the peak of the ester bond at 1720 cm<sup>-1</sup> increased, and the hydroxide radical content significantly decreased at 3440 cm<sup>-1</sup> in FTIR spectra [32, 33]. The results obtained from analysis

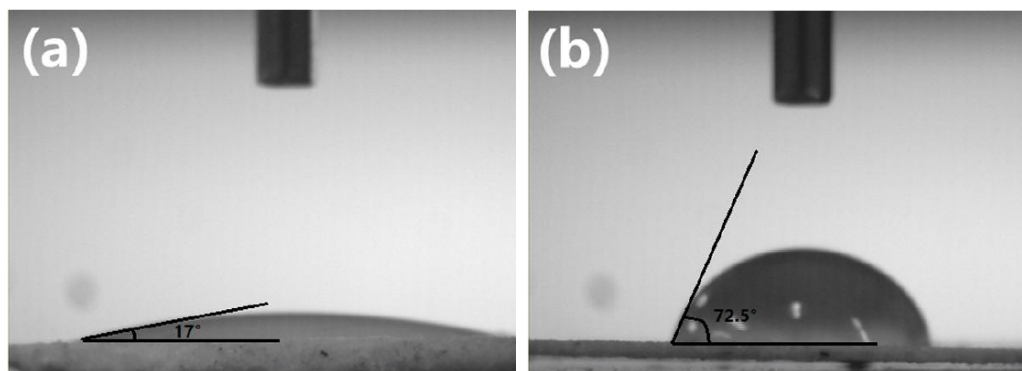


**Figure 2:** Photographs of contact angles for  $\beta$ -CD (a) and  $\beta$ -CD-PGMA (b).

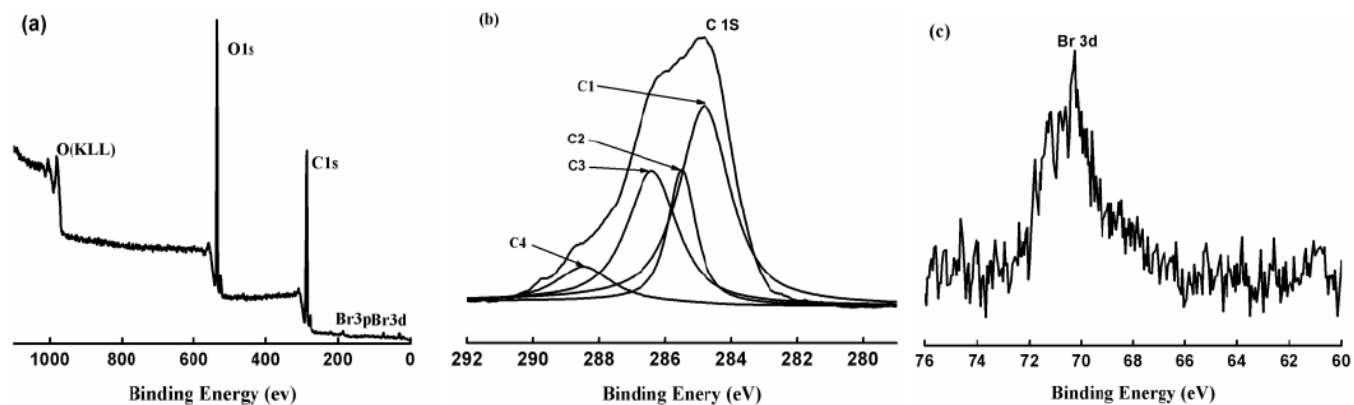


Figure 3: XPS spectra of  $\beta$ -CD-Br.

indicated that  $\beta$ -CD-PGMA star-shaped polymers could afford strong chemical adsorption and bonding interaction on the  $\beta$ -CD surface.

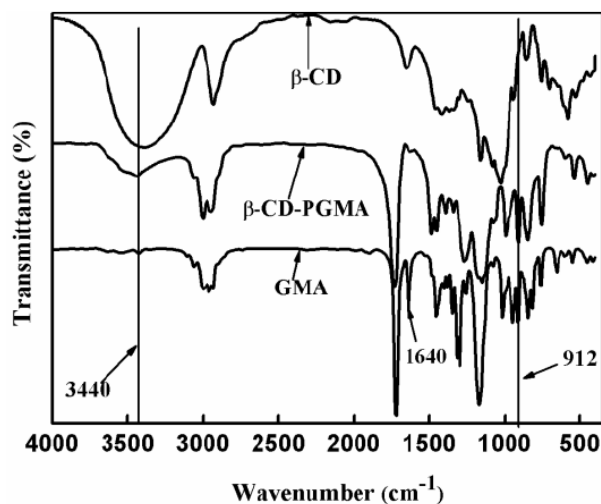


Figure 4: FTIR spectra of  $\beta$ -CD, GMA and  $\beta$ -CD-PGMA.

### 3.5. Raman Analysis

Figure 5 shows the Raman spectra of  $\beta$ -CD and  $\beta$ -CD-PGMA polymers. From Figure 5, in the spectra of  $\beta$ -CD-PGMA polymers, characteristic bands of  $\beta$ -CD were observed at 1260 and 950  $\text{cm}^{-1}$ , indicating that  $\beta$ -CD-PGMA star-shaped polymers contain the  $\beta$ -CD skeleton [34]. In the spectra of  $\beta$ -CD-PGMA, bands were observed at 1730, 1340, and 1132  $\text{cm}^{-1}$ , attributed to  $-\text{COO}-$ , saturated  $-\text{C}(\text{CH}_3)_2-$ , and backbone band of saturated fatty ether, respectively [35, 36]. The characteristic band of  $\beta$ -CD-PGMA was observed at 1640  $\text{cm}^{-1}$ , attributed to the ethylene  $\text{C}=\text{C}$  functional group of PGMA, indicating that the GMA monomer is grafted on  $\beta$ -CD via the opening of the double bond. In summary, the results obtained by Raman and IR spectra are consistent.

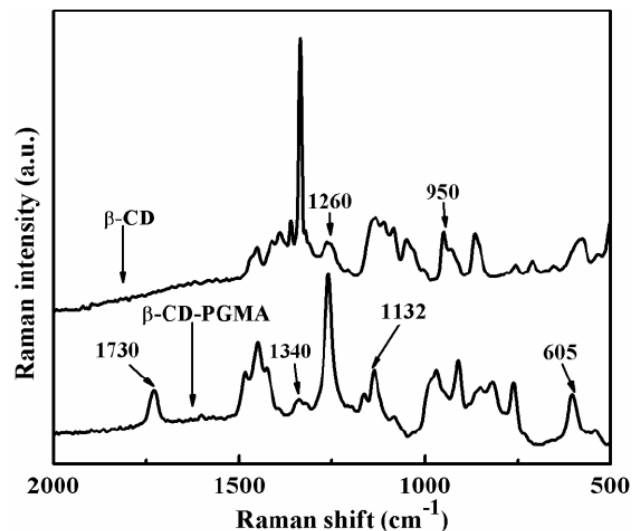


Figure 5: Raman spectra of  $\beta$ -CD-PGMA and  $\beta$ -CD.

### 3.6. $^1\text{H}$ NMR Analysis

Figure 6 shows the  $^1\text{H}$  NMR spectra of  $\beta$ -CD-PGMA star-shaped polymers, which characterized their chemical structure. A peak was observed at  $\delta = 1.89$  ppm, attributed to the methyl protons (**a**,  $\text{C}(\text{Br})\text{-CH}_3$ ) of the 2-bromoisobutyryl groups [13, 31]. Broad chemical shifts were observed in the  $\delta = 3.74$  ppm region, mainly attributed to the inner methyldyne and methylene protons between the oxygen and carbon moieties (**b**,  $\text{O-CH-C}$  and  $\text{O-CH}_2\text{-C}$ ) on the glucose units of  $\beta$ -CD. The peak at  $\delta = 4.83$  ppm was attributed to the inner methyldyne protons between the oxygen moieties (**b'**,  $\text{O-CHO}$ ).

Another peak was observed at  $\delta = 5.72$  ppm, corresponding to the hydroxyl protons adjacent to the methyldyne moieties (**c**,  $\text{CH-OH}$ ) of glucose units. Bands observed at 0.98–1.21 ppm were mainly attributed to the  $\text{C-CH}_3$  (**a'**) methyl protons of PGMA arms [5, 37]. The peaks observed at 1.82–2.0 ppm and

3.8–4.45 ppm were mainly attributed to the methylene protons C-CH<sub>2</sub> (d) and CH<sub>2</sub>-O-C=O (d') of PGMA arms, respectively. The peaks observed at 3.21 ppm and at approximately 2.66–2.85 ppm were mainly attributed to the hydrogen proton resonance peak in epoxy O-CH-C (b'') and O-CH<sub>2</sub>-C (b''') of PGMA arms, respectively. The signal associated with the CD core became less obvious, attributed to the minor contribution of CD to the overall star polymer structure [13]. From the peak area ratios of b''/b''', the molar ratio between the two was 118, which was close to the input ratio. Thus, the results obtained from <sup>1</sup>H NMR indicated that β-CD-PGMA star-shaped polymers are successfully prepared.

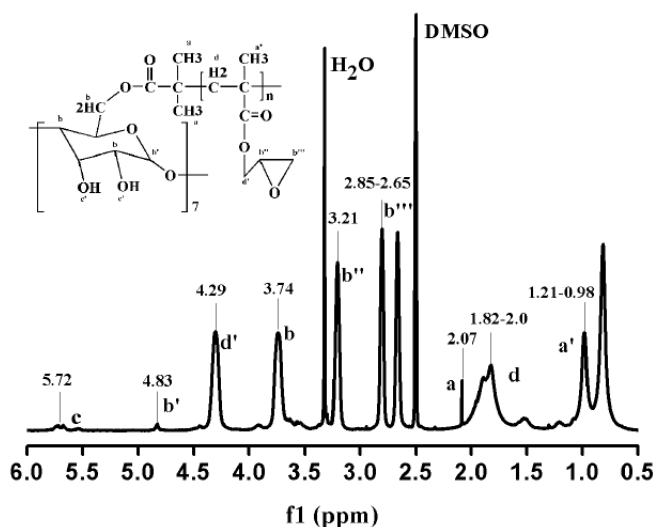


Figure 6: <sup>1</sup>H NMR spectrum of β-CD-PGMA.

### 3.7. Thermal Analysis

The thermal stability of a polymer is directly related to the polymer structure; hence, desirable information can be obtained with respect to regioselectivity [38]. Figure 7 shows the TGA curves of β-CD-PGMA in emulsion prepared via ATRP and pure β-CD. Pure β-CD and pristine homopolymer PGMA have been reported to be thermally stable up to 250 °C and 305 °C, respectively [10, 39]. However, the temperature at which β-CD-PGMA started to degrade was 147 °C, and the thermogram of β-CD-PGMA star-shaped polymers exhibited three degradation stages, with two major degradation stages at 316 °C and 402 °C. The first stage of degradation was observed from 147 °C to 255 °C, with a degradation rate of only 2.4 %; the degradation of this stage was attributed to the loss of loosely bound water molecules and the decomposition of epoxy groups associated to polymer moieties, as well as the ring opening of epoxy groups and formation of a few number of hydroxyl groups [37]. The second

stage of transition was observed from 255 °C to 344 °C, with a weight loss of 36.6 %, indicating that the β-CD core and a small amount of homopolymer PGMA are mainly degraded [10]. The third transition occurred from 344 °C to 481 °C with the loss of 60.9 %, attributed to the onset of the thermal degradation of PGMA arms. The increased degradation temperature of the β-CD-PGMA graft copolymer is attributed to the generation of random scission of the polymer chain by ATRP [38, 39]. Thus, this reaction is indicative of graft copolymerization, rather than homopolymerization of GMA.

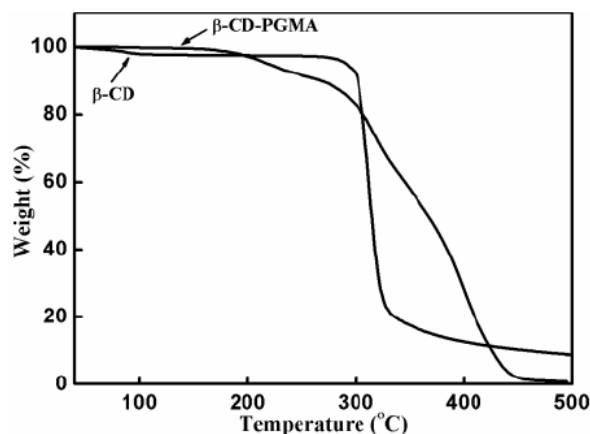


Figure 7: TG curves of β-CD-PGMA and β-CD.

The main thermal events in the DSC curves of polymeric products are melting and crystallization, which are observed in heating and cooling runs, respectively [3]. Figure 8 shows the DSC curves of β-CD-PGMA star-shaped polymers and pure β-CD. From Figure 8, the glass transition temperatures of β-CD and the PGMA block were 50 °C and 74 °C, respectively, and there was no crystallinity [40, 41]. Because of the formation of grafted PGMA and reduction of the relative content of β-CD, the glass temperature of β-CD at 50 °C is almost hidden [5]. However, the glass transition temperature of β-CD-PGMA star-shaped polymers was similar to that of homopolymer PGMA with increasing content of branched PGMA (>90 %). As compared with the glass transition temperature of the copolymer PGMA, that of β-CD-PGMA star-shaped polymers decreased, as shown in Figure 8, indicating that the reaction entails graft copolymerization rather than a mixture [30]. Two monomers were observed with no crystallinity, but the melting and crystallization peaks were observed in the DSC curve of β-CD-PGMA polymers, indicating that the crystallinity of star-shaped polymer material improved; this improvement may contribute to β-CD-Br as the initiator for the nucleating agent to induce the graft reaction of PGMA [3]. Thus,

the results obtained from TG and DSC indicated that  $\beta$ -CD-PGMA star-shaped polymers were successfully prepared.

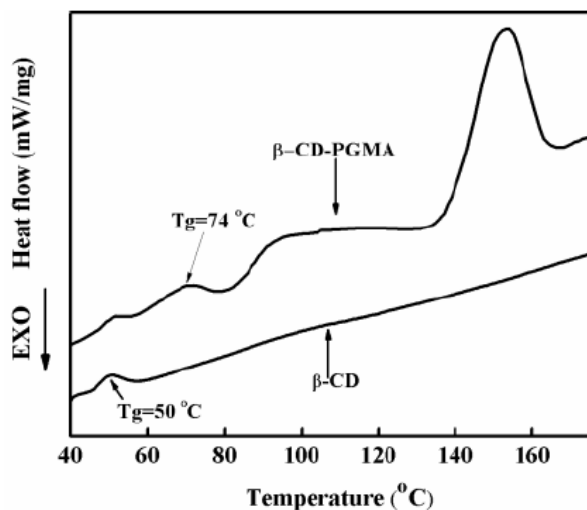


Figure 8: DSC curves of  $\beta$ -CD-PGMA and  $\beta$ -CD.

### 3.8. Structure and Properties of Phen/ $\beta$ -CD-PGMA Microspheres

#### 3.8.1. Orthogonal Optimization of Phen/ $\beta$ -CD-PGMA Microspheres

For optimizing the preparation of Phen/ $\beta$ -CD-PGMA microspheres, drug loading was utilized as the objective function. According to previously reported studies [11, 30], emulsion temperature is determined as room temperature, with a 5 mL emulsifier solution (volume ratio of [dichloromethane]/ [sulfoxide] of 9:1 (v:v)), and a water phase of 50 mL. The amount of  $\beta$ -CD-PGMA (A), dosage ratio of Phen and  $\beta$ -CD-PGMA (B), stirring speed (C) and water solution concentration of PVA (D) were selected as the four effect factors as the object of the orthogonal experiment. By the orthogonal design experiment of  $L_9 (3^4)$  (Table 3), the optimum conditions were selected, and then the Phen/ $\beta$ -CD-PGMA microspheres were prepared on the basis of the optimum conditions.

Table 3: Factor Level of the Orthogonal Experiment  $L_9 (3^4)$  of Phen/ $\beta$ -CD-PGMA Microspheres

Level	Factors			
	A (mg)	B (m/m)	C (r/min)	D (%)
1	100	1:2	600	1
2	200	1:4	900	2
3	300	1:8	1200	3

Table 4 shows the results obtained from the orthogonal experiments using  $\beta$ -CD-PGMA

microspheres. By the comparison of the range of each factor, factors that affect drug loading followed the sequence: dosage ratio of Phen and  $\beta$ -CD-PGMA (B) > stirring speed (C) > water solution concentration of PVA > amount of  $\beta$ -CD-PGMA (A). From Table 4, drug loading gradually increased with increasing loading amount of Phen in the microspheres. However, at a very high feed ratio, a small amount of small Phen particles was mixed in the drug-loaded microspheres. Stirring speed mainly affected the particle size of microspheres because high speed resulted in small particle size and less loading, which in turn induced the adhesion of microspheres. The PVA surfactant served to emulsify and disperse microspheres. The low PVA content possibly resulted in adhesion; conversely, the drug loading rate decreased while foaming and forming Phen micelles. In addition, with increasing dosage of  $\beta$ -CD-PGMA, microspheres caused adhesion. Besides, volatile  $\text{CH}_2\text{Cl}_2$  resulted in the collapse of the microspheres, leading to the rupture of microspheres and affecting the drug loading capacity.

Thus, results obtained from orthogonal experimental indicated that the optimum conditions for drug loading were a dosage ratio of 1:4 for Phen and  $\beta$ -CD-PGMA, a stirring speed of 900 rpm, a water solution concentration of PVA of 2 %, and the  $\beta$ -CD-PGMA amount of 200 mg. Finally, the drug loading of microspheres of Phen/ $\beta$ -CD-PGMA and Phen/ $\beta$ -CD under optimum conditions were 26.67 % and 5.51 %, respectively.

#### 3.8.2. FTIR Analysis of Microspheres

Figure 9 shows the FTIR spectra of Phen,  $\beta$ -CD-PGMA, and Phen/ $\beta$ -CD-PGMA. Absorption bands were observed at 1584, 1420 and 852  $\text{cm}^{-1}$ , attributed to the stretching vibration peak of the C=C skeleton on the aromatic ring, C–N stretching vibration and C–H bending vibration peak of the aromatic ring [30, 41], respectively. By contrast, the Phen/ $\beta$ -CD-PGMA curve also exhibited weak absorption peaks at 1420 and 852  $\text{cm}^{-1}$ . The results indicated that Phen is present in the microspheres, albeit in low content. No new characteristic absorption peaks were observed in the spectrum of Phen/ $\beta$ -CD-PGMA, indicating that no chemical reaction occurred between  $\beta$ -CD-PGMA and Phen.

#### 3.8.3. SEM Analysis of Microspheres

Figure 10 shows the SEM photographs of drug-loaded microspheres of Phen/ $\beta$ -CD and Phen/ $\beta$ -CD-PGMA microspheres after drug release. As shown in

Table 4: Results of Orthogonal Experiments of Phen/ $\beta$ -CD-PGMA Microspheres

No.	Factors				Drug loading (%)	Drug entrapment efficiency (%)
	A	B	C	D		
1	1	1	1	3	5.60	11.30
2	1	2	2	2	20.96	83.50
3	1	3	3	1	8.81	69.70
4	2	1	2	1	12.08	24.20
5	2	2	3	3	14.96	59.40
6	2	3	1	2	10.71	86.10
7	3	1	3	2	13.09	25.80
8	3	2	1	1	11.94	47.70
9	3	3	2	3	11.72	92.80
$K_1$	11.79	10.26	9.42	10.76		
$K_2$	12.58	15.95	14.92	14.92		
$K_3$	12.25	10.41	12.29	10.94		
$R$	0.79	5.69	5.50	4.16		

Effects of factors on experimental results: B > C > D > A; Optimum conditions: B<sub>2</sub>C<sub>2</sub>D<sub>2</sub>A<sub>2</sub>.

Figure 10a and 10b, under optimum conditions, drug-loaded microspheres were better, where the microsphere surface was spherical with relative smoothness and an average particle size of 10  $\mu$ m. On the other hand, as can be observed in Figure 10c and 10d, drug-loaded microspheres were broken and no longer exhibited a smooth surface, attributed to the fracture of the ester bonds in the graft and dissolution of CD. With increasing time release, the PBS solution entered into the microspheres and increased the contact between the solution and  $\beta$ -CD-PGMA microspheres, further accelerating the degradation of microspheres and drug release. Hence, SEM photographs completely illustrate that the sustained release of  $\beta$ -CD-PGMA is better than that of  $\beta$ -CD.

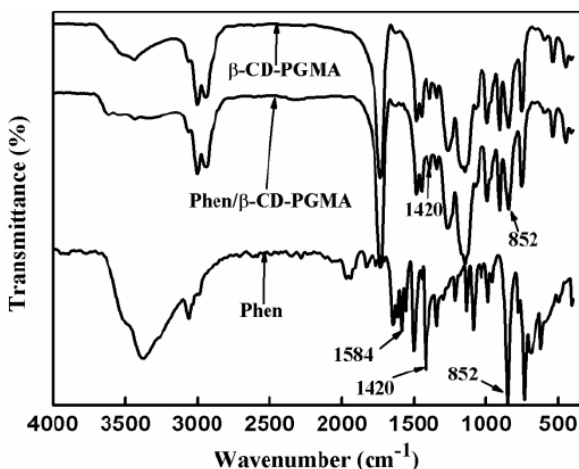
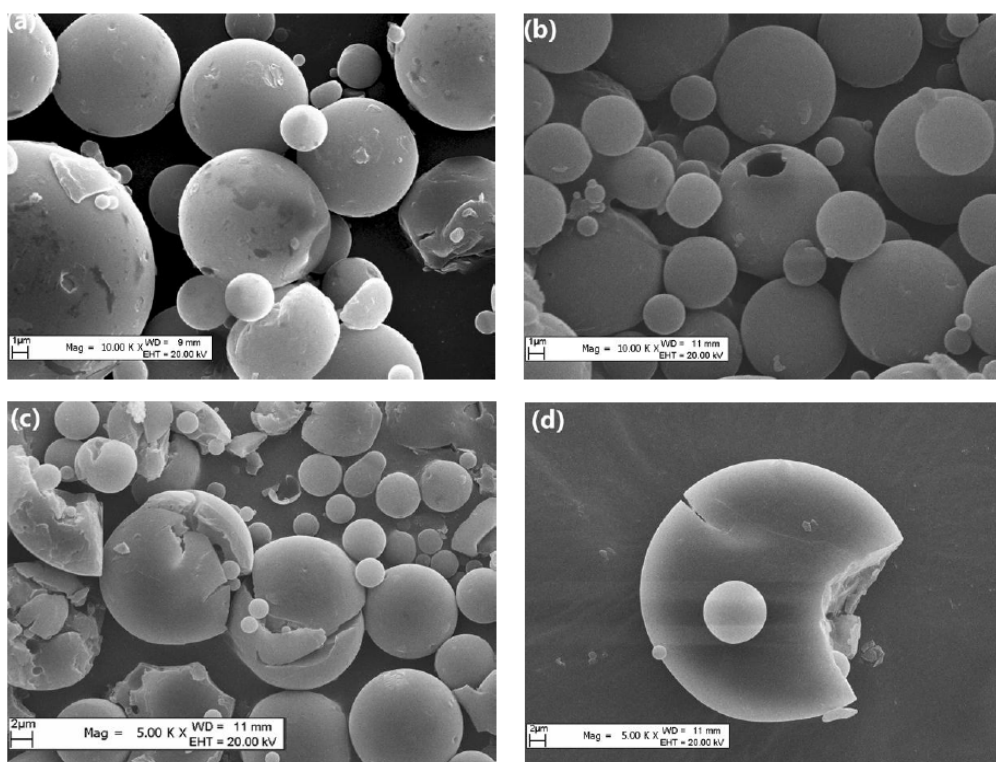


Figure 9: FTIR spectra of Phen,  $\beta$ -CD-PGMA, and Phen/ $\beta$ -CD-PGMA.

### 3.8.4. In Vitro Release Testing and Analysis

The release behavior of Phen from microspheres was investigated *in vitro* in a PBS solution (0.1 M, pH 7.4) at 37 °C by dynamic dialysis [5]. Figure 11 shows the *in vitro* release profile of Phen, Phen/ $\beta$ -CD, and Phen/ $\beta$ -CD-PGMA composite microspheres in PBS.

As observed in Figure 11, the release process of drug-loaded microspheres underwent three processes—swelling, stable and delayed release phases—with increasing time [42]. In the first 12 h, the drug release rates of pure Phen and Phen/ $\beta$ -CD were 72.9 % and 65.2 %, respectively, while the release of Phen/ $\beta$ -CD-PGMA microspheres was less than 38 %. Hence, the slow-release effect of  $\beta$ -CD-PGMA is better than that of  $\beta$ -CD and pure Phen. The first stage in the first 1 h corresponded to the swelling phase of drug-loaded microspheres, where microspheres were still in the contracted state, and the drug was not easily released from the contracted state of microspheres [43]. Simultaneously, the drug was mainly attributed to the phen on the surface of microspheres. The second stage, which lasted from 1 h to 24 h, was a relatively stable phase. In addition, with the swelling equilibrium, the microspheres were in complete contact with the solution, and the drug was smoothly released from microspheres [44]. After the end of this phase, the drug release rate of samples reached 94.4 %, 78.4 % and 49.3 %, respectively. After 72 h, the drug release rates of Phen/ $\beta$ -CD and Phen/ $\beta$ -CD-PGMA were 88.5 % and 60.9 %, respectively. In addition, although the drug



**Figure 10:** SEM images of microspheres: (a) Phen/ $\beta$ -CD drug-loaded microspheres; (b) Phen/ $\beta$ -CD-PGMA drug-loaded microspheres; (c) Phen/ $\beta$ -CD composite microspheres after drug release; (d) Phen/ $\beta$ -CD-PGMA microspheres after drug release.

continued to be released, release rate was difficult to meet the requirements for treatment. Thus, with respect to drug loading and drug release, drug-loaded microspheres of  $\beta$ -CD-PGMA are superior to drug-loaded microspheres of  $\beta$ -CD. Hence,  $\beta$ -CD-PGMA not only exhibits the drug release effect but also improves the drug utilization rate at a certain extent for controlling release.

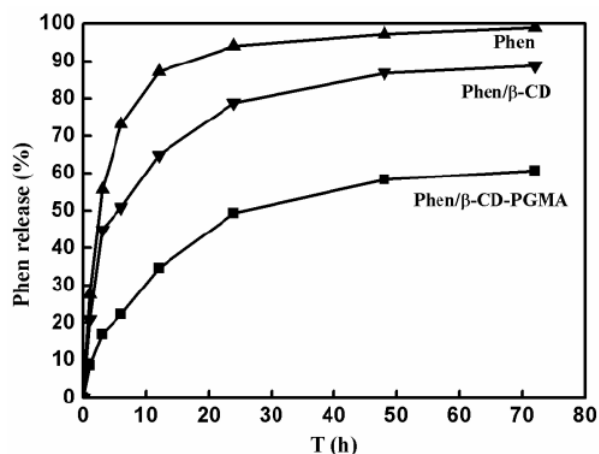


**Figure 11:** Drug release curves of Phen, Phen/ $\beta$ -CD-PGMA, and Phen/ $\beta$ -CD composite microspheres.

Taking into account the drug release kinetics of drug-loaded microspheres, the drug release curve of

the types of sustained-release microspheres *in vitro* was fitted with the zero-order equation, first-order kinetics equation, and Higuchi equation [43]. The fitting results indicated that the Higuchi equation well express the drug release characteristics of  $\beta$ -CD-PGMA in the first 48 h. Due to the fact that the value of 0.5 lies between 0.43 and 0.85, the mechanism was non-Fickian diffusion, where both drug diffusion and polymer relaxation determined the rate of drug release. Formula 4 shows the release kinetics equation of Phen/ $\beta$ -CD-PGMA microspheres.

$$y = 8.87t^{\frac{1}{2}} + 1.25, R^2 = 0.991 \quad (4)$$

#### 4. CONCLUSIONS

In this study,  $\beta$ -CD-PGMA star-shaped polymers, consisting of  $\beta$ -cyclodextrin and poly (glycidyl methacrylate), were synthesized by ATRP. The composition and structure of  $\beta$ -CD-PGMA star-shaped polymers thus obtained were confirmed by  $^1\text{H}$  NMR spectroscopy, FTIR, Raman, and XPS. TG and DSC analyses showed that the high content of PGMA in the copolymer resulted in the increase of the thermal degradation temperature and improvement of crystallinity. The hydrophilicity of  $\beta$ -CD-PGMA, as

compared with  $\beta$ -CD, obviously decreased. Based on SEM observations, these microspheres were spherical with a mean diameter of 10  $\mu$ m. Finally, the results obtained from a study for the release of Phen from these microspheres indicated that  $\beta$ -CD-GMA star-shaped polymers could be utilized for controlled drug delivery.

## ACKNOWLEDGMENTS

We greatly appreciate that this work is financially supported by National Science Foundation of China (51263019).

## REFERENCES

- [1] Saikia C, Hussain A, Ramteke A, Sharma HK, Deb P, Baji TK. Carboxymethyl starch-coated iron oxide magnetic nanoparticles: a potential drug delivery system for isoniazid. *Iran Polym J* 2015; 24: 815-28. <https://doi.org/10.1007/s13726-015-0370-z>
- [2] Chen WH, Luo GF, Lei Q, Cao FY, Fan JX, Qiu WX. Rational design of multifunctional magnetic mesoporous silica nanoparticle for tumor-targeted magnetic resonance imaging and precise therapy. *Biomaterials* 2016; 76: 87-101. <https://doi.org/10.1016/j.biomaterials.2015.10.053>
- [3] Sha K, Li DS, Li YP, Liu XT, Wang SW, Guan JQ, Wang JY. Synthesis, characterization, and micellization of an epoxy-based amphiphilic diblock copolymer of  $\epsilon$ -caprolactone and glycidyl methacrylate by enzymatic ring-opening polymerization and atom transfer radical polymerization. *J Appl Polym Sci A: Polym Chem* 2007; 45: 5037-49. <https://doi.org/10.1002/pola.22000>
- [4] Li JF, Yang HY, Zhang YJ, Jiang XT, Guo YB, An S, Ma HJ, He X, Jiang C. Choline derivate-modified doxorubicin loaded micelle for glioma therapy. *Acs Appl Mater Inter* 2015; 7: 21589-601. <https://doi.org/10.1021/acsami.5b07045>
- [5] Bagheri M, Motirasoul F. Synthesis, characterization, and micellization of cholesteryl-modified amphiphilic poly (L-lactide)-block-poly (glycidyl methacrylate) as a nanocarrier for hydrophobic drugs. *J Polym Res* 2013; 20: 1-9. <https://doi.org/10.1007/s10965-012-0059-3>
- [6] Nasr FH, Khoe S, Dehghan MM, Chaleshtori SS, Shafiee A. Preparation and evaluation of contact lenses embedded with polycaprolactone-based nanoparticles for ocular drug delivery. *Biomacromolecules* 2016; 17: 485-95. <https://doi.org/10.1021/acs.biomac.5b01387>
- [7] Canbolat MF, Celebioglu A, Uyar T. Drug delivery system based on cyclodextrin-naproxen inclusion complex incorporated in electrospun polycaprolactone nanofibers. *Colloids Surf B: Biointerfaces* 2014; 115: 15-21. <https://doi.org/10.1016/j.colsurfb.2013.11.021>
- [8] Weber LM, Lopez CG, Anseth KS. Effects of PEG hydrogel crosslinking density on protein diffusion and encapsulated islet survival and function. *J Biomed Mater Res A* 2009; 90: 720-29. <https://doi.org/10.1002/jbm.a.32134>
- [9] Hu JM, Zhang GY, Ge ZS, Liu SY. Stimuli-responsive tertiary amine methacrylate-based block copolymers: Synthesis, supramolecular self-assembly and functional applications. *Prog Polym Sci* 2014; 39: 1096-143. <https://doi.org/10.1016/j.progpolymsci.2013.10.006>
- [10] Aslan A, Çelik SÜ, Bozkurt A. Proton-conducting properties of the membranes based on poly (vinyl phosphonic acid) grafted poly (glycidyl methacrylate). *Solid State Ionics* 2009; 180: 1240-45. <https://doi.org/10.1016/j.ssi.2009.07.003>
- [11] Zhou WQ, Gu TY, Su ZG, Ma GH. Synthesis of macroporous poly (glycidyl methacrylate) microspheres by surfactant reverse micelles swelling method. *Eur Polym J* 2007; 43: 4493-502. <https://doi.org/10.1016/j.eurpolymj.2007.07.010>
- [12] Chung JE, Yokoyama M, Yamato M, Aoyagi T, Sakurai Y, Okano T. Thermo-responsive drug delivery from polymeric micelles constructed using block copolymers of poly (N-isopropylacrylamide) and poly (butylmethacrylate). *J Control Release* 1999; 62: 115-27. [https://doi.org/10.1016/S0168-3659\(99\)00029-2](https://doi.org/10.1016/S0168-3659(99)00029-2)
- [13] Xu FJ, Zhang ZX, Ping Y, Li J, Kang ET, Neoh KG. Star-shaped cationic polymers by atom transfer radical polymerization from  $\beta$ -cyclodextrin cores for nonviral gene delivery. *Biomacromolecules* 2009; 10: 285-93. <https://doi.org/10.1021/bm8010165>
- [14] Xu LJ, Liang XY, Zhang L, Wu JB, Li ZX, Yu MM, Wei LH. The vesicle formation of  $\beta$ -CD and AD self-assembly of dumbbell-shaped amphiphilic triblock copolymer. *Colloid Polym Sci* 2016; 294: 145-55. <https://doi.org/10.1007/s00396-015-3758-6>
- [15] Khodaverdi E, Aboumaashzadeh M, Tekie FSM, Hadizadeh F, Tabassi SAS, Mohajeri SA, Khashyarmansh Z, Haghghi HM. Sustained drug release using supramolecular hydrogels composed of cyclodextrin inclusion complexes with PCL/PEG multiple block copolymers. *Iran Polym J* 2014; 23: 707-16. <https://doi.org/10.1007/s13726-014-0265-4>
- [16] Gao H, Wang YN, Fan YG, Ma JB. Synthesis of a biodegradable tadpole-shaped polymer via the coupling reaction of polylactide onto mono (6-(2-aminoethyl) amino-6-deoxy)- $\beta$ -cyclodextrin and its properties as the new carrier of protein delivery system. *J Controlled Release* 2005; 107: 158-73. <https://doi.org/10.1016/j.jconrel.2005.06.010>
- [17] Khan AR, Forgo P, Stine KJ, Valerian. Methods for selective modifications of cyclodextrins. *Chem Rev* 1998; 98: 1977-96. <https://doi.org/10.1021/cr970012b>
- [18] Haroun AA, El-Halawany NR. Encapsulation of bovine serum albumin within  $\beta$ -cyclodextrin/gelatin-based polymeric hydrogel for controlled protein drug release. *IRBM* 2010; 31: 234-41. <https://doi.org/10.1016/j.irbm.2010.02.001>
- [19] Xin Y, Wang H, Liu BW, Yuan JY. Synthesis and MALDI-TOF characterization of  $\beta$ -CD core ATRP initiators and RAFT chain transfers with different degrees of substitution. *Chin J Polym Sci* 2015; 33: 36-48. <https://doi.org/10.1007/s10118-015-1572-8>
- [20] Shi HH, Lin CC. Photoclick hydrogels prepared from functionalized cyclodextrin and poly (ethylene glycol) for drug delivery and in situ cell encapsulation. *Biomacromolecules* 2015; 6: 1915-23. <https://doi.org/10.1021/acs.biomac.5b00471>
- [21] Huang Y, Fan XD. Synthesis and properties of hydrogels of poly (acrylic-co-acryloyl  $\beta$ -cyclodextrin). *J Appl Polym Sci* 2009; 113: 3068-77. <https://doi.org/10.1002/app.30259>
- [22] Georgiou TK, Vamvakaki M, Patrickios CS. Nanoscopic cationic methacrylate star homopolymers: synthesis by group transfer polymerization, characterization and evaluation as transfection reagents. *Biomacromolecules* 2004; 5: 2221-29. <https://doi.org/10.1021/bm049755e>
- [23] Paris R, Fuente JLDL. Synthesis of epoxy functionalized four-armed star diblock copolymers by atom transfer radical polymerization. *React Funct Polym* 2008; 68: 1004-12. <https://doi.org/10.1016/j.reactfunctpolym.2008.02.011>

- [24] Ren Q, Xiang YL, Huang CY, Li J, Wang CY. Epoxy-functionalized star-shaped polymers as novel tougheners for epoxy resin. *Polym Bull* 2015; 72: 2949-65. <https://doi.org/10.1007/s00289-015-1446-9>
- [25] Szejtli J. Introduction and general overview of cyclodextrin chemistry. *Chem Rev* 1998; 98: 1743-54. <https://doi.org/10.1021/cr970022c>
- [26] Haloi DJ, Mandal P, Singha NK. Atom transfer radical polymerization of glycidyl methacrylate (GMA) in emulsion. *J Macromol Sci A* 2013; 50: 121-27. <https://doi.org/10.1080/10601325.2013.736270>
- [27] Sun Y, Du H, Lan Y. Preparation and properties of fluorinated amphiphilic copolymers via iron-mediated AGET ATRP. *Iran Polym J* 2015; 24: 95-103. <https://doi.org/10.1007/s13726-014-0303-2>
- [28] Li RQ, Niu YL, Zhao NN, Yu BR, Mao C, Xu FJ. Series of New  $\beta$ -Cyclodextrin-Cored Starlike Carriers for Gene Delivery. *ACS Appl Mater Inter* 2014; 6: 3969-78. <https://doi.org/10.1021/am5005255>
- [29] Xu FJ, Wang ZH, Yang WT. Surface functionalization of polycaprolactone films via surface-initiated atom transfer radical polymerization for covalently coupling cell-adhesive biomolecules. *Biomaterials* 2010; 31: 3139-47. <https://doi.org/10.1016/j.biomaterials.2010.01.032>
- [30] Zhang YZ, Li HQ, Li H, Li R, Xiao CF. Preparation and characterization of modified polyvinyl alcohol ultrafiltration membranes. *Desalination* 2006; 192: 214-23. <https://doi.org/10.1016/j.desal.2005.07.037>
- [31] Xu FJ, Li H, Li J, Zhang ZX, Kang ET, Neoh KG. Pentablock copolymers of poly (ethylene glycol), poly ((2-dimethyl amino) ethyl methacrylate) and poly (2-hydroxyethyl methacrylate) from consecutive atom transfer radical polymerizations for non-viral gene delivery. *Biomaterials* 2008; 29: 3023-33. <https://doi.org/10.1016/j.biomaterials.2008.03.041>
- [32] Hu XT, Wei BX, Li HY, Wu CS, Bai YX, Xu XM, Jin ZY, Tian YQ. Preparation of the  $\beta$ -cyclodextrin-vitamin C ( $\beta$ -CD-Vc) inclusion complex under high hydrostatic pressure (HHP). *Carbohydr Polym* 2012; 90: 1193-96. <https://doi.org/10.1016/j.carbpol.2012.06.029>
- [33] Li QL, Wang LZ, Qiu XL, Sun YL, Wang PX, Liu Y, Li F, Qi AD, Gao H, Yang YW. Stimuli-responsive biocompatible nanovalves based on  $\beta$ -cyclodextrin modified poly (glycidyl methacrylate). *Polym Chem* 2014; 5: 3389-95. <https://doi.org/10.1039/c4py00041b>
- [34] Iliescu T, Baia M, Miclăuș V. A raman spectroscopic study of the diclofenac sodium- $\beta$ -cyclodextrin interaction. *Eur J Pharm Sci* 2004; 22: 487-95. <https://doi.org/10.1016/j.ejps.2004.05.003>
- [35] Li QQ, Du YP, Tang HR, Wang X, Chen GP, Iqbal J, Wang WM, Zhang WB. Ultra sensitive surface-enhanced Raman scattering detection based on monolithic column as a new type substrate. *J Raman Spectrosc* 2012; 43: 1392-96. <https://doi.org/10.1002/jrs.4095>
- [36] Zou Y, Armstrong SR, Jessop JLP. Apparent conversion of adhesive resin in the hybrid layer, Part 1: identification of an internal reference for raman spectroscopy and the effects of water storage. *J Biomed Mater Res A* 2008; 86: 883-91. <https://doi.org/10.1002/jbm.a.31684>
- [37] Xu Y, Yuan J, Müller AHE. Single-molecular hybrid nanocylinders: Attaching polyhedral oligomeric silsesquioxane covalently to poly (glycidyl methacrylate) cylindrical brushes. *Polymer* 2009; 50: 5933-39. <https://doi.org/10.1016/j.polymer.2009.10.029>
- [38] Krishnan R, Srinivasan KSV. Room temperature atom transfer radical polymerization of glycidyl methacrylate mediated by copper (I)/N-alkyl-2-pyridylmethanimine complexes. *Macromolecules* 2004; 37: 3614-22. <https://doi.org/10.1021/ma0359032>
- [39] Nanjundan S, Unnithan CS, Selvamalar CSJ, Penlidis A. Homopolymer of 4-benzoylphenyl methacrylate and its copolymers with glycidyl methacrylate: synthesis, characterization, monomer reactivity ratios and application as adhesives. *React Funct Polym* 2005; 62: 11-24. <https://doi.org/10.1016/j.reactfunctpolym.2004.08.006>
- [40] Pralhad T, Rajendrakumar K. Study of freeze-dried quercetin-cyclodextrin binary systems by DSC, FT-IR, X-ray diffraction and SEM analysis. *J Pharm Biomed Anal* 2004; 34: 333-39. [https://doi.org/10.1016/S0731-7085\(03\)00529-6](https://doi.org/10.1016/S0731-7085(03)00529-6)
- [41] Çelik SÜ, Bozkurt A. Preparation and proton conductivity of acid-doped 5-aminotetrazole functional poly (glycidyl methacrylate). *Eur Polym J* 2008; 44: 213-18. <https://doi.org/10.1016/j.eurpolymj.2007.10.010>
- [42] Chen FM, Wu ZF, Sun HH, Wu H, Xin SN. Release of bioactive BMP from dextran-derived microspheres: a novel delivery concept. *Int J Pharm* 2006; 307: 23-32. <https://doi.org/10.1016/j.ijpharm.2005.09.024>
- [43] Anirudhan TS, Divya PL, Nima J. Synthesis and characterization of novel drug delivery system using modified chitosan based hydrogel grafted with cyclodextrin. *Chem Eng J* 2016; 284: 1259-69. <https://doi.org/10.1016/j.cej.2015.09.057>
- [44] Anirudhan TS, Divya PL, Nima J. Synthesis and characterization of silane coated magnetic nanoparticles/glycidylmethacrylate-grafted-maleated cyclodextrin composite hydrogel as a drug carrier for the controlled delivery of 5-fluorouracil. *Mater Sci Eng C* 2015; 55: 471-81. <https://doi.org/10.1016/j.msec.2015.05.068>